AGU PUBLICATIONS

JGR

Journal of Geophysical Research: Atmospheres

RESEARCH ARTICLE
10.1002/2015JD024718

Key Points:
- The importance of black carbon (BC) geometry on its optical properties is stressed
- Sensitivities of BC Ångström exponent (AE) are numerically studied
- The AE becomes more sensitive to particle size as BC geometry becomes compact

Correspondence to:
C. Liu,
chao_liu@nuist.edu.cn

Citation:
Li, J., C. Liu, Y. Yin, and K. R. Kumar (2016), Numerical investigation on the Ångström exponent of black carbon aerosol, *J. Geophys. Res. Atmos.*, *121*, 3506–3518, doi:10.1002/2015JD024718.

Received 1 JAN 2016
Accepted 16 MAR 2016
Accepted article online 23 MAR 2016
Published online 6 APR 2016

Numerical investigation on the Ångström exponent of black carbon aerosol

Ji Li[1,2], Chao Liu[1,2], Yan Yin[1,2], and K. Raghavendra Kumar[2]

[1]Collaborative Innovation Center on Forecast and Evaluation of Meteorological Disasters, Nanjing University of Information Science and Technology, Nanjing, China, [2]Key Laboratory for Aerosol-Cloud-Precipitation of China Meteorological Administration, School of Atmospheric Physics, Nanjing University of Information Science and Technology, Nanjing, China

Abstract Black carbon (BC) plays an important role on the global and regional climate, whereas there are significant uncertainties on its optical properties. Among various optical properties, the Ångström exponent (AE) indicates the spectral variation of the particle-optic interaction and is widely used to understand the aerosol properties. We consider the influence of BC geometry on its optical properties and assess the sensitivity of the AE to particle geometry and size distribution. The fractal aggregates with different fractal dimensions are used to represent realistic BC particles, and popular equivalent volume spherical and spheroidal models are also considered for comparison. Even if the fractal aggregates become highly compact and spherical, their optical properties are still significantly different from those of equivalent volume spheres or spheroids. Meanwhile, the Rayleigh-Debye-Gans approximation can hardly provide accurate results for all optical quantities of aggregates with different dimensions. The extinction Ångström exponent (EAE) and absorption Ångström exponent (AAE) are sensitive to both particle geometry and size distribution. With BC becoming more compact (from fractal aggregate to spheroid and to sphere), the AE becomes more sensitive to particle size distribution. The EAE and AAE of aggregates with different size distributions vary between 1.10–1.63 and 0.87–1.50, respectively, whereas those of the spheres or spheroids have wider ranges. Furthermore, the AE at smaller wavelengths (between 0.35 μm and 0.55 μm) is more sensitive to geometry and size distribution than that given by optical properties at larger wavelengths (between 0.55 μm and 0.88 μm).

1. Introduction

Black carbon (BC or soot), released from incomplete combustion of fossil fuel, biofuel, and biomass, is one of the strongest absorptive aerosols of solar radiation and plays a critical role on global and regional climate [*Jacobson*, 2001; *Bond and Sun*, 2005; *Chakrabarty et al*., 2009; *Scarnato et al*., 2013]. BC can both warm the lower atmosphere by absorption and reduce the solar radiation reaching the surface [*Hansen et al*., 1997; *Kaufman et al*., 2002], whereas the lack of accurate understanding and parameterization on BC wavelength-dependent optical properties has become a key limitation on assessing its radiative effects [*Bond and Bergstrom*, 2006; *Bond et al*., 2013; *Pandey et al*., 2015; *Smith et al*., 2015]. Furthermore, aerosol absorption and scattering properties are fundamental for a variety of applications, such as optical diagnostics of industrial aerosol processes and combustion, environmental problems (e.g., visibility and haze), and remote sensing [*Sorensen*, 2001; *Kaufman et al*., 2002; *Mishchenko et al*., 2004; *Liu and Mishchenko*, 2005; *Yin and Liu*, 2010; *Liu and Smallwood*, 2010; *Yi et al*., 2014].

It is well known that the optical properties of BC particles are substantially influenced by their microphysical properties, e.g., geometry and size distribution [*Chakrabarty et al*., 2006; *Liu and Mishchenko*, 2007; *Li et al*., 2010]. The fractal aggregate, which shows excellent similarity to the realistic BC aggregates, is the most widely accepted numerical geometry used to simulate BC optical properties. In addition, observations indicate that BC aggregates fold up from chain-like clusters into more spherical ones during a very short period of time [*Martins et al*., 1998; *Smith and Grainger*, 2014]. During the aging process, BC might also be coated by water or other nucleating byproducts of burning (such as sulphate and organic carbon). Thus, more and more sophisticated geometric models are developed to study the optical properties of those nonspherical and inhomogeneous BC particles [*Chung et al*., 2011; *Dong et al*., 2015]. For homogeneous cases, the aggregates with overlapping or dispersal monomers have been considered [*Bescond et al*., 2014; *Liu et al*., 2015]. To account for the coating effects, a few complicated models with different mixing structures were built [*Liu et al*., 2012; *Scarnato et al*., 2013; *Dong et al*., 2015]. Most of those studies found that the optical properties of BC were sensitive to particle geometry and even some detailed structures. Meanwhile, due to the simplicity

and high efficiency for optical property simulation, equivalent sphere is always the most popular model for applications such as radiation transfer and remote sensing, although the corresponding optical properties can be significantly different from those of BC with more realistic geometries [*Li et al*., 2010; *Dong et al*., 2015].

Among the various optical properties, the Ångström exponent (AE) indicates the relative strengths of extinction or absorption at different wavelengths and has been widely used to infer aerosol size and type. The AE is originally introduced in the Ångström power law to express the optical depth of different wavelengths [*Ångström*, 1929], i.e.,

$$\tau_\lambda = b\lambda^{-\alpha}, \tag{1}$$

where τ_λ is the optical thickness at the wavelength of λ, α is the Ångström exponent (AE), and b is a constant independent of wavelength. Following the above general expression, the extinction Ångström exponent (EAE) and absorption Ångström exponent (AAE) are similarly defined to indicate the wavelength dependence of aerosol extinction and absorption [*Lewis et al*., 2008]:

$$C_{\text{ext}}(\lambda) = b_{\text{ext}}\lambda^{-\text{EAE}}, \tag{2}$$

$$C_{\text{abs}}(\lambda) = b_{\text{abs}}\lambda^{-\text{AAE}}. \tag{3}$$

Here $C_{\text{ext}}(\lambda)$ and $C_{\text{abs}}(\lambda)$ are the extinction and absorption cross sections at the wavelength of λ. Thus, if the extinction and absorption cross sections at two wavelengths are known, the EAE and AAE can be approximated by

$$\text{EAE} = -\frac{\ln(C_{\text{ext1}}/C_{\text{ext2}})}{\ln(\lambda_1/\lambda_2)}, \tag{4}$$

and

$$\text{AAE} = -\frac{\ln(C_{\text{abs1}}/C_{\text{abs2}})}{\ln(\lambda_1/\lambda_2)}, \tag{5}$$

where C_{ext1} and C_{ext2} are the extinction cross sections at the wavelengths of λ_1 and λ_2, respectively, and C_{abs1} and C_{abs2} are the corresponding absorption cross sections. The EAE is an indicator of the predominant aerosol size, because the spectral shape of the extinction is related to the particle size [*Eck et al*., 1999; *Schuster et al*., 2006; *Toledano et al*., 2007]. Thus, it can be used to distinguish fine- and coarse-mode aerosol particles [*Toledano et al*., 2007]. The AAE, describing the absorption variation at different wavelengths, is also used for aerosol classification [*Russell et al*., 2010; *Schuster et al*., 2015]. For example, the small-sized strong absorptive BC particles are typically assumed to have AAE around 1 at visible and near-infrared wavelengths [*Scarnato et al*., 2013; *Schuster et al*., 2015], and the brown carbon, which absorbs much more radiation with shorter wavelengths (UV), has much larger AAE (normally larger than 3) [*Yang et al*., 2009]. The AE was extensively used to analyze the measured optical properties in previous studies [*Toledano et al*., 2007; *Russell et al*., 2010; *Soni et al*., 2011]. The Aerosol Robotic Network measurements as well as other experimental results use the EAE and AAE as key parameters to understand aerosol properties [*Toledano et al*., 2007; *Russell et al*., 2010; *Smith et al*., 2015]. Furthermore, the EAE/AAE is also widely applied for numerical studies on estimating aerosol radiative forcing [*Reid et al*., 1999; *Chung et al*., 2011].

As discussed above, significant numerical investigations have been carried out to study the optical properties of BC (e.g., extinction, scattering and absorption cross sections, single-scattering albedo, and phase function) at a certain (single) wavelength, whereas few research focuses on theoretical investigation of its AE [*Scarnato et al*., 2013], and it significantly limits our ability to understand the measurements and to carry out accurate radiative transfer simulations. Thus, a systematic numerical investigation on the AE of BC aerosols is necessary and meaningful to understand the aerosol optical measurement and will benefit the radiative transfer simulations and remote sensing applications.

To further improve our understanding on the AE of BC aerosols, this paper numerically investigates the importance of BC geometry and size distribution on its optical properties at three wavelengths (UV-VIS-NIR), and the sensitivity of the AE is systematically stressed. The aggregates with different fractal dimensions, equivalent volume sphere, and spheroid are considered, and their optical properties are simulated using the Multiple Sphere T-Matrix (MSTM), Rayleigh-Debye-Gans (RDG), and Lorenz-Mie and T-matrix methods. The particle geometries as well as the scattering models applied are discussed in section 2, and section 3 provides the

details on calculating the bulk scattering properties. Section 4 illustrates our results by comparing the BC optical properties based on different geometries and size distributions. Section 5 concludes this work.

2. Methodology: BC Geometries and Scattering Simulations

Observations indicate that BC particles normally exist in the form of cluster-like aggregates containing numerous similar-sized spherical monomers, and the "fractal aggregate" shows great success on describing their aggregation geometry [*Köylü et al*., 1995a; *Sorensen*, 2001; *Scarnato et al*., 2013]. Mathematically, the fractal aggregate obeys the statistical scaling rule [*Sorensen*, 2001]:

$$N = k_f \left(\frac{R_g}{a}\right)^{D_f} \tag{6}$$

where N is the number of monomers in an aggregate and a is the monomer radius. k_f and D_f are the fractal prefactor and fractal dimension, respectively, and they indicate the overall structure of the aggregates. The aggregate tends to be more compact as D_f or k_f increases. For example, a D_f of 1 corresponds to aggregate with a loose chain-like structure, and compact aggregates have D_f close to 3 [*Smith and Grainger*, 2014]. R_g, a measure of the aggregate overall spatial dimension, is the radius of gyration, and it can be calculated by

$$R_g^2 = \frac{1}{N}\sum_{i=1}^{N}(\mathbf{r_i} - \mathbf{r}_0)^2, \tag{7}$$

where $\mathbf{r_i}$ is the position vector of the ith monomer center and $\mathbf{r}_0$ indicates the position vector of the aggregate mass center.

The fractal dimension and fractal prefactor are two key parameters to characterize fractal-like aggregates [*Köylü et al*., 1995b; *Sorensen and Roberts*, 1997; *Brasil et al*., 2000]. Both theoretical and experimental studies have been carried out to evaluate k_f and D_f of BC aggregates [*Schnaiter et al*., 2005; *Liu and Mishchenko*, 2005; *Chakrabarty et al*., 2014]. Because the BC may not only come from various sources (e.g., industry, power generation, residential, and transportation) [*Streets et al*., 2001] but also undergo different atmospheric aging processes and durations [*Kouji et al*., 2007], the aggregates were observed to have fractal dimensions ranging from 1.9 to 2.6 [*Chakrabarty et al*., 2006]. Fresh BC particles with very loose structure generally have fractal dimensions less than 2. During the aging process, the chain-like aggregates tend to collapse into more compact clusters, and thus, the fractal dimension D_f becomes larger, i.e., being close to 3 [*Liu et al*., 2008]. The change on aggregation geometry through aging is expected to have an important effect on their optical properties, and numerical studies have clearly shown the influence [*Liu and Mishchenko*, 2005].

Multiple numerical models are available to simulate the optical properties of aggregates with small spherical monomers. Numerically exact methods include the MSTM method [*Liu et al*., 2008; *Mackowski and Mishchenko*, 2011], the generalized multiparticle Mie method [*Xu*, 1995; *Liu et al*., 2013], and the discrete dipole approximation [*Kimura*, 2001]. Those numerical exact methods require accurate particle geometries and large computational resources and, thus, show limited application on atmospheric researches. Considering the significant variation on BC geometries and the computational burden, even highly simplified parameterization of their optical properties could be challenging for practical applications [*Smith and Grainger*, 2014]. As a result, approximated methods such as the RDG method show wide applications due to its high efficiency [*Sorensen*, 2001; *Liu et al*., 2013]. This study uses both an exact model, i.e., the MSTM, and the RDG approximation to simulate the optical properties of aggregates.

The MSTM, an accurate numerical model, calculates the scattering properties of a cluster of spherical particles within the framework of the T-matrix method. It can obtain the T-matrix of multiple spheres from the T-matrices of individual spheres by employing the addition theorem of vector spherical wave functions to account for mutual interaction among the system [*Mackowski and Mishchenko*, 1996], and all information required for particle scattering and absorption properties can be derived from its T-matrix. The popular and robust MSTM code developed and published by *Mackowski and Mishchenko* [2011] has been widely applied to obtain the optical properties of fractal aggregates [*Liu and Mishchenko*, 2005, 2007; *Smith and Grainger*, 2014; *Liu et al*., 2015] and is used in this study. Meanwhile, the RDG assumes the monomers to be Rayleigh scatterers and ignores the intercluster multiple scattering [*Sorensen*, 2001; *Liu et al*., 2008]. The RGD gives aggregate absorption by direct summation of those of single monomers, and the scattering is

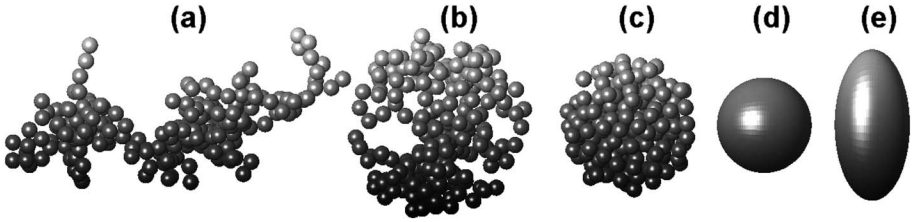

Figure 1. Examples of modeled black carbon geometries. (a–c) Fractal aggregates containing 200 monomers with fractal dimensions of 1.8, 2.4, and 2.8, (d) equivalent volume sphere, and (e) equivalent volume spheroid (aspect ratio of 2), whose volumes are equal to that of the aggregates with 200 monomers.

approximated by considering scattering of individual monomers and a scattering factor. Thus, it gives really simple expressions for the optical properties of aggregates and can be applied efficiently without specific aggregate realizations (only using the geometric parameters). The details on the RDG and its formulas can be found in the classic review given by *Sorensen* [2001].

Spherical approximations based on different equivalent quantities (volume and surface) were found to produce poor agreement on the phase functions of aggregates with a fractal dimension of 1.82 [*Li et al*., 2010; *Smith and Grainger*, 2014], whereas only the loose aggregates (D_f up to 2.25) were verified and compared. As aggregates become compact and spherical, the performance of spherical approximation is still an open question. To represent BC aggregates at different aging stages and structures, i.e., both loose and compact aggregates, the fractal dimensions D_f from 1.8 to 2.8 in steps of 0.2 are considered. The fractal prefactor has less significant influence on aggregate geometry and also shows less variation. As a result, the fractal prefactor is fixed to be constants, and widely accepted values of $k_f = 1.20$ are used [*Liu et al*., 2008, 2013; *Dong et al*., 2015]. Furthermore, we use a fixed monomer radiance of $a = 0.015$ μm. A tunable particle-cluster aggregation algorithm is applied to generate fractal aggregates [*Filippov et al*., 2000]. Figures 1a–1c show examples of BC fractal aggregates with three different fractal dimensions (i.e., 1.8, 2.4, and 2.8), and the dramatic changes due to the increase of D_f are clearly shown. Each aggregate in the figure contains 200 monomers.

Spheres are the simplest three-dimensional geometry used to model the optical properties of aerosol particles, and spheroids show great success on various applications related to optical properties of dust particles [*Mishchenko et al*., 1997; *Dubovik et al*., 2006; *Yi et al*., 2011]. Thus, equivalent volume spheres and equivalent volume spheroids are also used in this study, and their accuracy can be determined by comparing with those of more realistic aggregates. Considering that spheroidal soot particles were also observed [*Ueda et al*., 2011], the spherical and spheroidal models can serve not only as simplified approximations for BC but also as the actual representation of realistic BC particles [*Mishchenko et al*., 2013]. For an aggregate with N monomers, the radius of the equivalent volume sphere is given by $a\sqrt[3]{N}$. Prolate spheroids with an aspect ratio of 2 are assumed, and the short and long axis corresponding to an aggregate with N monomers are $a\sqrt[3]{N/2}$ and $2a\sqrt[3]{N/2}$, respectively. The equivalent volume sphere and spheroid corresponding to an aggregate with 200 monomers are given in Figures 1d and 1e. The Lorenz-Mie and T-matrix methods are employed to calculate the optical properties of spheres and spheroids [*Mie*, 1908; *Mishchenko and Travis*, 1998; *Yang et al*., 2015], and they are the most fundamental and classic models for the corresponding particles. In summary, a total of eight geometries, i.e., fractal aggregates with six different fractal dimensions and equivalent volume sphere and spheroid, are considered in our study, and two methods (an accurate and an approximated one) are used for the optical properties of aggregates.

To demonstrate the relative computational burden of the models discussed above, we give an example here. It should be known that the Lorenz-Mie theory is a highly efficient model for light scattering by a single sphere, and it takes less than 1 s for any particle considered in this study with a single processor (64 bits 2.5 GHz). The RGD, an approximation based on the Rayleigh approximation, takes even less computational resource than the Lorenz-Mie method. However, with the same processor, the MSTM takes approximately 100 s for an aggregate with 200 monomers and $D_f = 1.8$ at the wavelength of 0.55 μm, and multiple aggregates (at least five) with different realizations but the same size (N) (at least five) should be considered to give reliable averaged properties. More computational time is needed as aggregate becomes larger or wavelength becomes smaller.

As a result, although giving the exact optical properties, the MSTM method may become unpractical for atmospheric applications.

3. Bulk Optical Properties

For atmospheric applications, only the bulk optical properties averaged over a certain particle size distribution are meaningful, and all results shown in this study are ensemble-averaged properties. The radii of the equivalent volume spheres are assumed to follow a lognormal size distribution in the form of

$$n(r) = \frac{1}{\sqrt{2\pi}r\ln(\sigma_g)}\exp\left[-\left(\frac{\ln(r)-\ln(r_g)}{\sqrt{2}\ln(\sigma_g)}\right)^2\right], \tag{8}$$

where r_g and σ_g are the geometric mean radius and geometric standard deviation, respectively. To assess the sensitivity of the EAE and AAE to particle size distribution, r_g ranging from 0.025 μm to 0.075 μm is considered, and σ_g ranges from 1.1 to 2.0. With the particle size distribution given, the bulk scattering properties can be easily given by the following equations:

$$\langle C_{\text{ext}}\rangle = \int_{r_{\min}}^{r_{\max}} C_{\text{ext}}(r)n(r)\mathrm{d}(r) \tag{9}$$

$$\langle C_{\text{abs}}\rangle = \int_{r_{\min}}^{r_{\max}} C_{\text{abs}}(r)n(r)\mathrm{d}(r) \tag{10}$$

$$\langle \text{SSA}\rangle = \frac{\langle C_{\text{sca}}\rangle}{\langle C_{\text{ext}}\rangle} \tag{11}$$

$$\langle g\rangle = \frac{\int_{r_{\min}}^{r_{\max}} g(r)C_{\text{sca}}(r)n(r)\mathrm{d}(r)}{\int_{r_{\min}}^{r_{\max}} C_{\text{sca}}(r)n(r)\mathrm{d}(r)} \tag{12}$$

and

$$\langle P(\theta)\rangle = \frac{\int_{r_{\min}}^{r_{\max}} P(\theta,r)C_{\text{sca}}(r)n(r)\mathrm{d}r}{\int_{r_{\min}}^{r_{\max}} C_{\text{sca}}(r)n(r)\mathrm{d}r} \tag{13}$$

The minimum and maximum equivalent volume radii are $r_{\min} = 0.015$ μm and $r_{\max} = 0.15$ μm, respectively. The bulk scattering properties calculated above include the extinction cross section (C_{ext}), the absorption cross section (C_{abs}), single-scattering albedo (SSA), asymmetry factor (g), and phase function $P(\theta)$. With the ensemble-averaged properties obtained, it is straight forward to give the EAE and AAE following equations (4) and (5). It should be noticed that all optical properties discussed in this study are those of randomly oriented particles, which can be given analytically by the MSTM, RDG, and T-matrix methods.

The AE of BC aerosols indicates the spectral variation of particle extinction and absorption, and the wavelengths and refractive indices chosen would certainly influence our results. Three wavelengths of 0.35 μm, 0.55 μm, and 0.88 μm are considered, and the corresponding complex refractive indices are 1.64–0.67i, 1.73–0.59i, and 1.80–0.57i following *Chang and Charalampopoulos* [1990]. With optical properties at three wavelengths, two AE results are calculated and discussed: values with subscribe "1" (e.g., EAE_1 and AAE_1) refer to results based on BC extinctions and absorptions at wavelengths of 0.35 μm and 0.55 μm (following equations (4) and (5)) and "2" is used for values between larger wavelengths of 0.55 μm and 0.88 μm. It should be noticed that with significant uncertainties in the BC refractive indices [*Chang and Charalampopoulos*, 1990; *Ayranci et al.*, 2007], our results and conclusions are specified for BC with the above mentioned refractive indices. However, we focus only on the effects of BC geometry and size distribution, and the variation on BC refractive index would not qualitatively change our conclusions.

4. Results and Discussions

4.1. Optical Properties at a Single Wavelength

Table 1 compares the bulk optical properties of BC with different geometries at a wavelength of 0.55 μm. As discussed in the previous section, fractal aggregates with six different D_f from 1.8 to 2.8, equivalent volume spheres, and spheroids are considered. The averaged extinction and absorption cross sections

Table 1. Extinction Cross Section (C_{ext}), Absorption Cross Section (C_{abs}), Single-Scattering Albedo (SSA), and Asymmetry Factor (g) of Fractal Aggregates With Different D_f and Equivalent Volume Sphere and Spheroid at a Wavelength of 0.55 μm[a]

Geometry		C_{ext} ($\times 10^{-2}$ μm^2)	C_{abs} ($\times 10^{-2}$ μm^2)	SSA	g
Aggregate D_f	1.8	1.72 (1.50)	1.52 (1.34)	0.12 (0.11)	0.54 (0.56)
	2.0	1.75 (1.57)	1.51 (1.34)	0.14 (0.15)	0.58 (0.55)
	2.2	1.78 (1.65)	1.50 (1.34)	0.16 (0.19)	0.61 (0.52)
	2.4	1.84 (1.75)	1.49 (1.34)	0.19 (0.24)	0.60 (0.49)
	2.6	1.92 (1.86)	1.49 (1.34)	0.22 (0.28)	0.56 (0.44)
	2.8	2.02 (1.97)	1.51 (1.34)	0.25 (0.32)	0.50 (0.39)
Equivalent volume sphere		2.38	1.66	0.30	0.34
Equivalent volume spheroid		2.43	1.72	0.29	0.35

[a]For fractal aggregates, the values outside the parentheses are given by the MSTM and those inside the parentheses are given by the RDG.

(C_{ext} and C_{abs}), single-scattering albedo (SSA), and asymmetry factor (g) per particle are listed in Table 1. The properties are averaged over an ensemble of particles with a typical BC size distribution, i.e., a lognormal size distribution with r_g of 0.06 μm and σ_g of 1.5 [*Alexander et al.*, 2008; *Chung et al.*, 2011]. For fractal aggregates, the values outside parentheses are given by the MSTM and those inside parentheses are given by the RDG. The C_{ext} given by the MSTM and RDG methods increases by 17% and 31%, respectively, when D_f increases from 1.8 to 2.8. Even if the aggregates with D_f of 2.8 are highly compact and spherical (see Figure 1c), the C_{ext} of equivalent volume spheres and spheroids are still at least 17% and 20% larger than that of the aggregates. However, the C_{abs} of aggregates with different D_f shows less differences, and the values given by the MSTM are larger than those computed by the RDG. Similar to the extinction, the absorptions of equivalent volume spheres and spheroids are larger than those of aggregates by over 10%. With the given extinction and absorption cross sections, it should be expected that the SSA of aggregates increases as the geometry becomes more compact, and those of spheres and spheroids are also much larger. The g of aggregates given by the MSTM does not show monotonic change as D_f increases, whereas the values given by the RDG decrease. Our results are generally consistent with those of a single-sized aggregate [*Liu and Mishchenko*, 2008]. In brief, two important conclusions can be drawn from the table. First, when the structure of fractal aggregates becomes more compact and spherical, i.e., with D_f increasing, their optical properties become close to those of equivalent volume spheres and spheroids. However, the values based on spherical and spheroidal particles still show significant differences from those of aggregates, and this is a valuable addition to the previous study given by *Li et al.* [2010] and *Smith and Grainger* [2014]. Thus, no matter how compact the aggregates become, significant errors would be introduced if BC particles were treated as spheres or spheroids. Second, the errors introduced by the RDG approximation can be comparable to those based on spherical or spheroidal approximations. Similar results are obtained for the optical properties at wavelengths of 0.35 μm and 0.88 μm, and thus, their values are not listed in the table.

To show a clearer comparison on the bulk optical properties of BC with different geometries, Figure 2 illustrates all the values given in Table 1 as well as those at the other two wavelengths. The results of aggregates are illustrated as functions of fractal dimension. Considering that aggregates of different fractal dimensions correspond to the same equivalent volume spheres or spheroids, results based on spheres and spheroids are expressed by the horizontal lines in the figure. The C_{ext} and C_{abs} decrease dramatically as the wavelength increases, i.e., positive EAE or AAE. The C_{ext} of fractal aggregates at 0.35 μm is over 3 times larger than that at 0.88 μm. The relative differences between the C_{ext} of aggregates (accurate results given by the MSTM) and spheres/spheroids are generally under 5% at the wavelength of 0.35 μm, whereas significant bias (over 10%) is noticed for the extinction and absorption at the other two wavelengths. At all three wavelengths, the SSA of aggregates increases as the fractal dimension increases, and the aggregates with $D_f = 2.8$ show relatively close SSAs (relative differences around 10%) to those of spheres or spheroids. The g given by the RDG approximation and the MSTM shows better agreement for aggregates with small fractal dimensions (1.8 and 2.0), and the RDG underestimates g as aggregate becomes compact. The equivalent volume sphere and spheroid underestimate the g of aggregates with different dimensions at all three wavelengths. In conclusion, the RDG approximation, which shows acceptable performance for

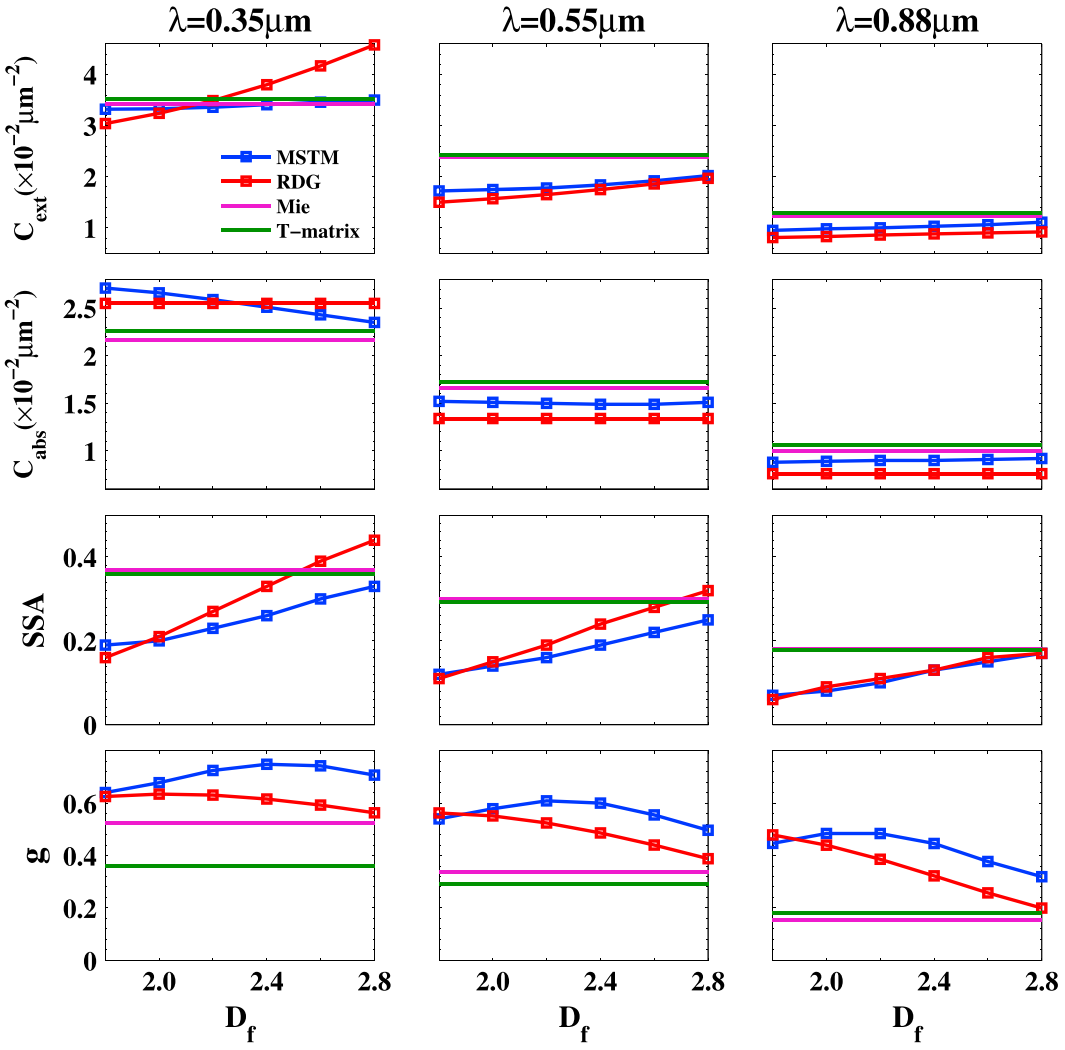

Figure 2. Extinction cross section (C_{ext}), absorption cross section (C_{abs}), single-scattering albedo (SSA), and asymmetry factor (g) per particle for black carbon with different geometries at three wavelengths of 0.35 μm, 0.55 μm, and 0.88 μm.

some quantities at some wavelengths, can hardly provide accurate results of all properties over all fractal dimensions. Meanwhile, the optical properties of equivalent volume spheres and spheroids differ from those of aggregates significantly. Thus, the realistic aggregate structure as well as accurate optical models has to be used to consider the optical properties of those particles.

Figure 3 shows the phase functions (P_{11}) of BC particles with different geometries, i.e., aggregates of three different dimensions (1.8, 2.4, and 2.8), equivalent volume spheres, and spheroids, at three wavelengths (from upper to lower panels). The phase function shown in the figure is normalized to satisfy $\frac{1}{2}\int_0^\pi P(\theta)\sin\theta d\theta = 1$. The same particle size distribution as used for previous simulations is considered. Figure 3 (left column) illustrates the phase functions of aggregates given by the MSTM and those of spheres and spheroids, and Figure 3 (right column) compares the results given by the MSTM and the RDG. The forward scattering calculated by the MSTM decreases with D_f increasing. The equivalent volume sphere and spheroid show similar phase functions at all three wavelengths (in Figure 3, left column), whereas, compared with those of aggregates, neither is close to those of aggregates. Figure 3 (right column) shows the performance of the RDG approximation on evaluating the phase function of aggregates. For small D_f (= 1.8), P given by the RDG shows close agreement with that given by the MSTM. However, as D_f becomes larger, the differences between the two methods become obvious. The forward scattering given by the RDG is smaller than the MSTM results, and the backward scattering of the RDG method is stronger than those from the MSTM method.

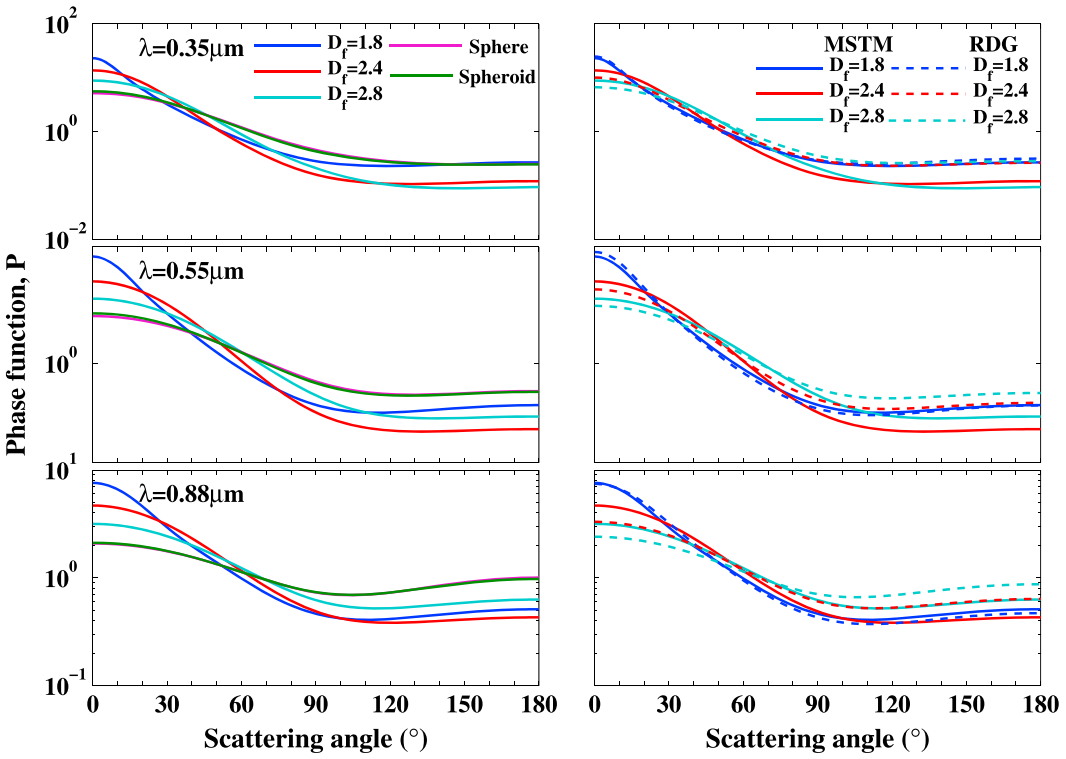

Figure 3. Normalized phase functions (P_{11}) of black carbon with different geometries given by different numerical models at three wavelengths (0.35 μm, 0.55 μm, and 0.88 μm).

4.2. Ångström Exponent

Previous table and figures illustrate the optical properties of BC at three independent wavelengths, and the AEs are discussed in this subsection. Figure 4 shows the EAE (top row) and AAE (bottom row) of BC particles with the aforementioned size distribution. All the data in the figure are also listed in Table 2. Again, for fractal aggregate, the values given by the MSTM and RDG are listed outside and inside the parentheses, respectively. The EAE_1 given by the MSTM decreases from 1.45 to 1.21 as the aggregate gets compact, and the EAE_2 shows slight variation between 1.28 and 1.33. However, the EAE_1 and EAE_2 values computed by the RDG increase by approximately 20% as D_f increases from 1.8 to 2.8. The different trends of the EAE given by the two methods show the limitation of the RDG approximation on the spectral varying optical properties. This may be due to the nature of the RDG approximation, which ignores the interaggregate multiple scattering, so the relative errors of the RDG may increase as particle becomes more compact, i.e., D_f increases. The MSTM and the RDG methods both give the EAE larger than 1, whereas the EAE_1 of equivalent volume sphere and spheroid is smaller than that of fractal aggregates (only around 0.8). The EAE_2 of equivalent volume sphere and spheroid are close to those of aggregates given by the MSTM and the RDG, and the relative differences are less than 15%. Overall, the BC aggregates with a loose chain structure have larger AAE than the compact ones, which agrees with previous observations and simulations [*Reid et al*., 1999; *Scarnato et al*., 2013]. The AAE_1 given by the MSTM is in the range between 0.98 and 1.28, and the AAE_2 varies from 1.05 to 1.15. The AAE computed by the RDG is a constant for different D_f, because the absorption given by the RDG is independent of BC aggregation (just a sum of monomer absorptions). The AAE_1 of equivalent volume sphere and spheroid are much smaller than those of aggregates, whereas the AAE_2 of BC with all different geometries have relatively close values between 1.0 and 1.2. Generally, the AEs between the wavelengths of 0.35 μm and 0.55 μm are more sensitive to BC geometries, and the results based on different geometries show significant differences. As the wavelength becomes larger, the AE becomes less sensitive to particle geometry. This is because the particle size parameter corresponding to longer wavelengths is relatively smaller, and the influence of particle geometry on their optical properties becomes weaker (e.g., Rayleigh scattering is independent of particle geometry.)

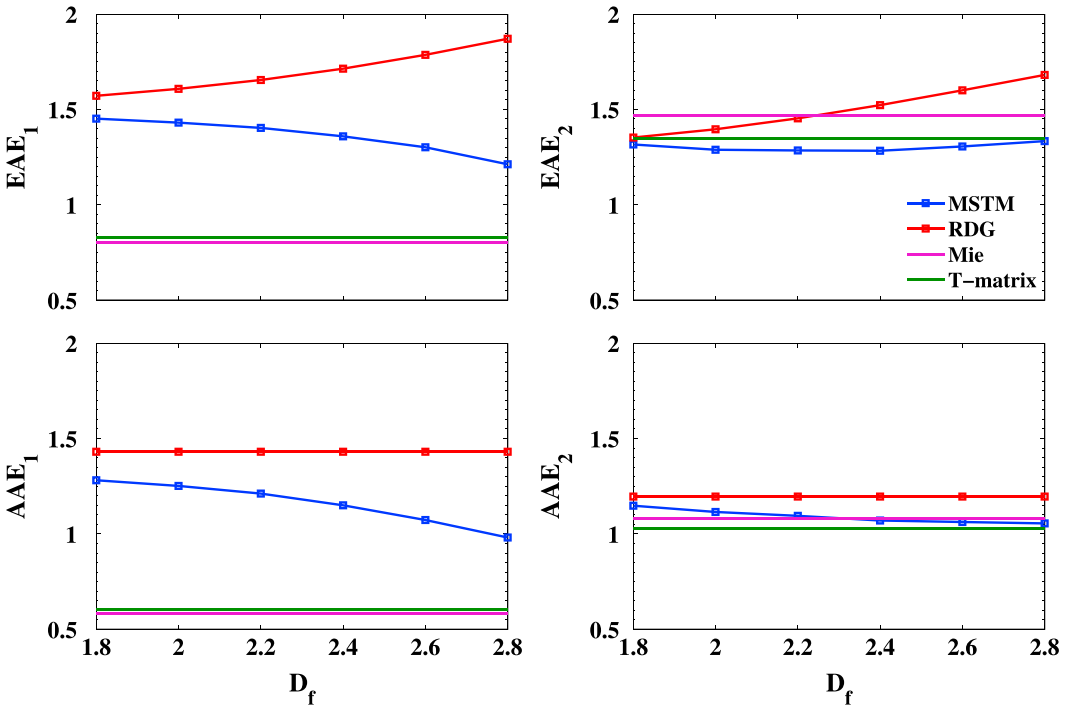

Figure 4. (top row) Extinction Ångström exponent (EAE) and (bottom row) absorption Ångström exponent (AAE) for BC particles with different geometries.

Figure 5 illustrates the variation of EAE with different particle size distribution, and the four panels from left to right correspond to four geometries: aggregates with $D_f = 1.8$ and 2.8, sphere, and spheroid. The results of aggregates are calculated by the exact MSTM method. Figure 5 shows the EAE_1 (top row) and the EAE_2 (bottom row), respectively. The lognormal size distributions are assumed for the BC particles with r_g (x axis) ranging from 0.025 μm to 0.075 μm and σ_g (y axis) ranging from 1.1 to 2.0. Figure 5 clearly shows that the EAE is quite sensitive to both particle size distribution and geometry. The EAE_1 decreases as r_g or σ_g increases, i.e., particle becoming larger or size distribution becoming wider. For the fractal aggregates with $D_f = 1.8$, the EAE_1 is in a range between 1.43 and 1.54 and shows weak variation on particle size distribution. However, the variation of EAE_1 becomes stronger as the aggregate becomes more compact with a fractal dimension of 2.8, and its values vary from 1.10 to 1.63. The EAE_1 of the equivalent spheres and spheroids at different size distributions shows similar variations and close values, and the relative differences are less than 8%. Comparing the results of all four geometries, the EAE_1 becomes more sensitive to the particle size distribution, i.e., showing larger variation, as particle geometry becomes more compact (from loose aggregate to compact aggregate, to spheroid, and to sphere), and the spheres give the largest range of the EAE_1 from

Table 2. Extinction Ångström Exponent (EAE) and Absorption Ångström Exponent (AAE) of Black Carbon Based on Different Geometries[a]

Geometry		EAE_1	EAE_2	AAE_1	AAE_2
Aggregate D_f	1.8	1.45 (1.57)	1.32 (1.35)	1.28 (1.43)	1.15 (1.20)
	2.0	1.43 (1.60)	1.29 (1.40)	1.25 (1.43)	1.12 (1.20)
	2.2	1.40 (1.65)	1.28 (1.45)	1.21 (1.43)	1.09 (1.20)
	2.4	1.36 (1.71)	1.28 (1.52)	1.15 (1.43)	1.07 (1.20)
	2.6	1.30 (1.79)	1.31 (1.60)	1.07 (1.43)	1.06 (1.20)
	2.8	1.21 (1.87)	1.33 (1.68)	0.98 (1.43)	1.05 (1.20)
Equivalent volume sphere		0.80	1.47	0.58	1.08
Equivalent volume spheroid		0.83	1.35	0.60	1.03

[a]For fractal aggregates, the values outside and inside the parentheses are those given by the MSTM and RDG, respectively.

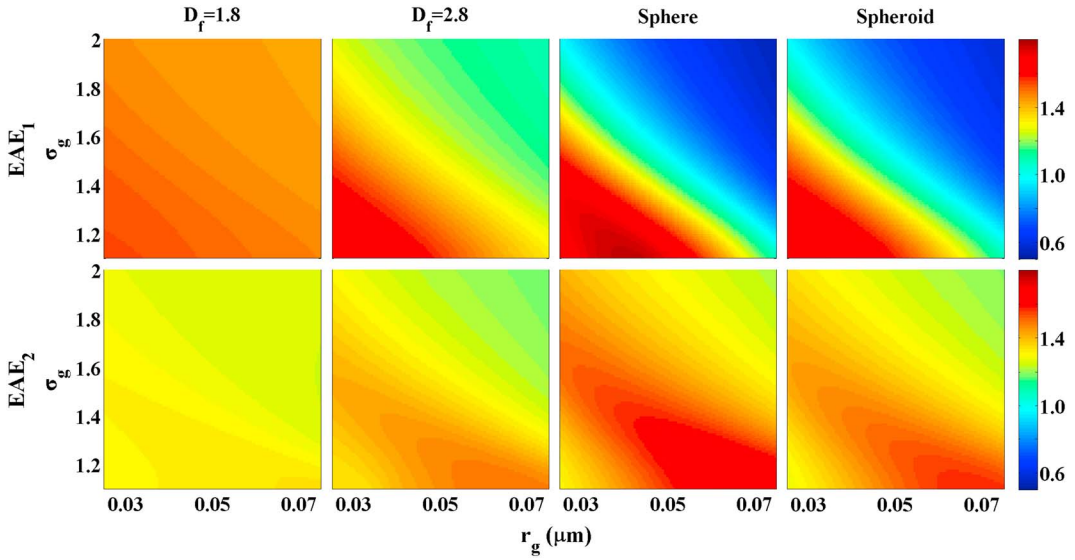

Figure 5. Extinction Ångström exponent (EAE) of fractal aggregates with D_f of 1.8 and 2.8, equivalent volume sphere, and spheroid with different particle size distributions.

0.54 to 1.77. In Figure 5 (bottom row), the EAE_2 shows similar patterns to those of the EAE_1, whereas the variation on particle size distribution becomes more complicated. Compared to the EAE_1, the EAE_2 has much narrower range for all four geometries, e.g., from 1.20 to 1.70 for spheres. Overall, Figure 5 indicates that the EAE are both sensitive to particle geometry and size distribution, and the sensitivity of the EAE to particle size distribution becomes stronger as particle becomes more compact and wavelength becomes smaller. However, the optical properties are highly complicated functions of particle size, shape, and refractive index, and this becomes more significant for the EAE, which is affected by relative properties (i.e., ratio of the extinctions) of multiple wavelengths. Thus, the conclusion given in this study should be carefully verified before being applied for other cases.

Similar to Figure 5, the AAE_1 and AAE_2 values are shown in Figure 6. The variations of the AAE are similar to those of the EAE. For loose aggregates with $D_f = 1.8$, the AAE_1 is in a range between 1.25 and 1.45, and the AAE_2 is smaller. When D_f is increased to 2.8, the AAE_1 can be as small as 0.86 for large BC particles, i.e., large

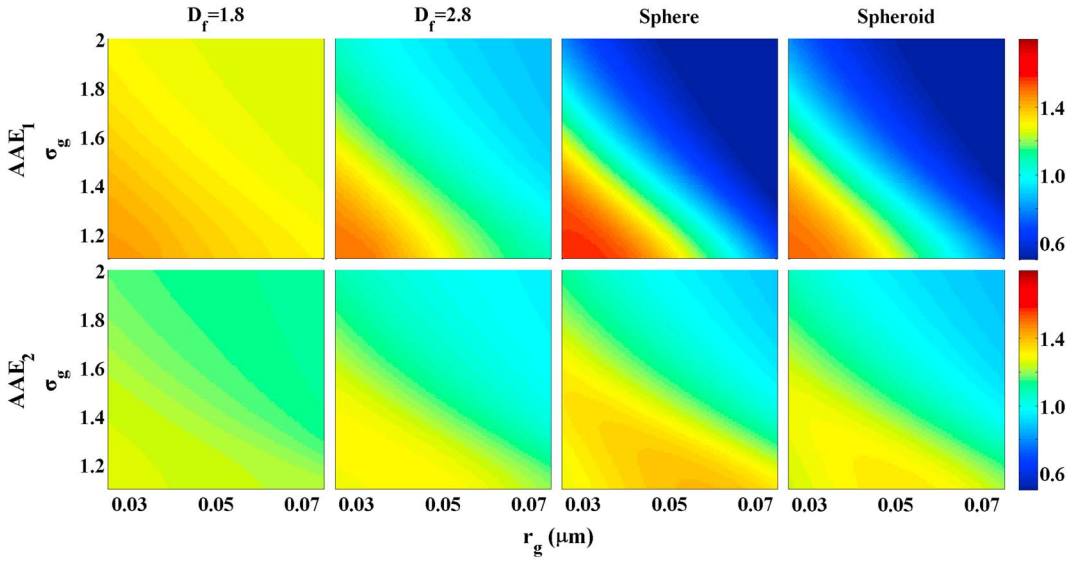

Figure 6. The same as in Figure 5 but for the absorption Ångström exponent (AAE).

r_g. Again, the AAE_1 of equivalent volume sphere has the widest range between 0.36 and 1.57, and those of the spheroids are similar with relative differences less than 9%. The variation of the AAE_2 is similar to that of the AAE_1, whereas its values become less sensitive to the particle geometry and size distribution. For the absorption, the AE given by the equivalent volume spheres or spheroids becomes closer to those of aggregates, especially the highly compact aggregates, whereas the difference between the AAEs of aggregates and spheres can still be over 50%.

5. Conclusion

This study explores the impact of geometry and size distribution on the optical properties of BC particles, especially on the AE. The fractal aggregate is applied to model the realistic BC geometry, and their optical properties are calculated using the numerically exact MSTM method and the RDG approximation. The equivalent volume sphere and spheroid (with an aspect ratio of 2) are also considered for comparison, because they are the simplest and most widely used geometries for atmospheric aerosols. Our results indicate that both geometry and size distribution have significant effects on the optical properties of BC particles. The RDG approximation shows limited accuracy in estimating the optical properties of BC aggregates. The equivalent volume spheres and spheroids have quite similar bulk optical properties, whereas they are quite different from those of fractal aggregates, even from those with highly compact structure. The EAE and AAE are sensitive to both BC geometry and size distribution, and as particle becomes more compact (from loose aggregate to sphere), the sensitivity of the AE to BC size distribution becomes stronger. Meanwhile, the AE also becomes less sensitive to the geometry and size distribution as the wavelength becomes larger. Again, the equivalent volume sphere and spheroid models may introduce significant errors if they are used to approximate the AE of BC aerosols. In conclusion, both accurate geometry and accurate scattering model should be used to account for BC rigorous optical properties. Because of the computation burden, more complete database or parameterization of the BC optical properties (such as that give by *Smith and Grainger* [2014]) should be developed in further studies for radiative transfer simulations and remote sensing.

Acknowledgments

We particularly thank Daniel W. Mackowski for the MSTM code (http://eng.auburn.edu/users/dmckwski/scatcodes/) and Michael I. Mishchenko for the T-matrix code (http://www.giss.nasa.gov/staff/mmishchenko/t_matrix.html). All data related to this work are available from the authors upon request (chao_liu@nuist.edu.cn). This work is financially supported by the National Natural Science Foundation of China (NSFC) (grant 41505018, 41571348, and 41590873), the Natural Science Foundation of Jiangsu Province (grant BK20150899), and the China Meteorological Administration R&D Special Fund for Public Welfare (Meteorology) (grant GYHY201506002).

References

Alexander, D. T., P. A. Crozier, and J. R. Anderson (2008), Brown carbon spheres in East Asian outflow and their optical properties, *Science*, *321*(5890), 833–836.

Ångström, A. (1929), On the atmospheric transmission of Sun radiation and on dust in the air. I and II, *Geogr. Ann.*, *11*, 156–166.

Ayranci, I., R. Vaillon, N. Selçuk, F. André, and D. Escudié (2007), Determination of soot temperature, volume fraction and refractive index from flame emission spectrometry, *J. Quant. Spectrosc. Radiat. Transfer*, *104*(2), 266–276.

Bescond, A., J. Yon, F. X. Ouf, D. Ferry, D. Delhaye, D. Gaffié, and C. Rozé (2014), Automated determination of aggregate primary particle size distribution by TEM image analysis: Application to soot, *Aerosol Sci. Technol.*, *48*(8), 831–841.

Bond, T. C., and H. Sun (2005), Can reducing black carbon emissions counteract global warming?, *Environ. Sci. Technol.*, *39*(16), 5921–5926.

Bond, T. C., and R. W. Bergstrom (2006), Light absorption by carbonaceous particles: An investigative review, *Aerosol Sci. Technol.*, *40*(1), 27–67.

Bond, T. C., S. J. Doherty, D. W. Fahey, P. M. Forster, T. Berntsen, B. J. DeAngelo, and C. S. Zender (2013), Bounding the role of black carbon in the climate system: A scientific assessment, *J. Geophys. Res. Atmos.*, *118*, 5380–5552, doi:10.1002/jgrd.50171.

Brasil, A. M., T. L. Farias, and M. G. Carvalho (2000), Evaluation of the fractal properties of cluster—Cluster aggregates, *Aerosol Sci. Technol.*, *33*(5), 440–454.

Chakrabarty, R. K., H. Moosmüller, M. A. Garro, W. P. Arnott, J. Walker, R. A. Susott, and W. M. Hao (2006), Emissions from the laboratory combustion of wildland fuels: Particle morphology and size, *J. Geophys. Res.*, *111*, D07204, doi:10.1029/2005JD006659.

Chakrabarty, R. K., et al. (2009), Low fractal dimension cluster-dilute soot aggregates from a premixed flame, *Phys. Rev. Lett.*, *102*(23), 235504.

Chakrabarty, R. K., N. D. Beres, H. Moosmüller, S. China, C. Mazzoleni, M. K. Dubey, L. Liu, and M. I. Mishchenko (2014), Soot superaggregates from flaming wildfires and their direct radiative forcing, *Sci. Rep.*, *4*, 5508, doi:10.1038/srep05508.

Chang, H., and T. T. Charalampopoulos (1990), Determination of the wavelength dependence of refractive indices of flame soot, *Proc. R. Soc. Lond. A*, *430*, 577–591.

Chung, C. E., K. Lee, and D. Müller (2011), Effect of internal mixture on black carbon radiative forcing, *Tellus B*, *64*(1), 1–13.

Dong, J., J. M. Zhao, and L. H. Liu (2015), Morphological effects on the radiative properties of soot aerosols in different internally mixing states with sulfate, *J. Quant. Spectrosc. Radiat. Transfer*, *165*, 43–55.

Dubovik, O., et al. (2006), Application of spheroid models to account for aerosol particle nonsphericity in remote sensing of desert dust, *J. Geophys. Res.*, *111*, D11208, doi:10.1029/2005JD006619.

Eck, T. F., B. N. Holben, J. S. Reid, O. Dubovik, A. Smirnov, N. T. O'neill, and S. Kinne (1999), Wavelength dependence of the optical depth of biomass burning, urban, and desert dust aerosols, *J. Geophys. Res.*, *104*(D24), 31,333–31,349, doi:10.1029/1999JD900923.

Filippov, A. V., M. Zurita, and D. E. Rosner (2000), Fractal-like aggregates: Relation between morphology and physical properties, *J. Colloid Interf. Sci.*, *229*(1), 261–273.

Hansen, J., M. Sato, and R. Ruedy (1997), Radiative forcing and climate response, *J. Geophys. Res.*, *102*, 6831–6864, doi:10.1029/96JD03436.

Jacobson, M. Z. (2001), Strong radiative heating due to the mixing state of black carbon in atmospheric aerosols, *Nature*, *409*(6821), 695–697.

Kaufman, Y. J., D. Tanré, and O. Boucher (2002), A satellite view of aerosols in the climate system, *Nature*, *419*(6903), 215–223.

Kimura, H. (2001), Light-scattering properties of fractal aggregates: Numerical calculations by a superposition technique and the discrete-dipole approximation, *J. Quant. Spectrosc. Radiat. Transfer*, *70*(4), 581–594.

Kouji, A., S. H. Chung, F. Heiner, and P. R. Buseck (2007), Fractal parameters of individual soot particles determined using electron tomography: Implications for optical properties, *J. Geophys. Res.*, *112*, D14202, doi:10.1029/2006JD008296.
Köylü, Ü. Ö., G. M. Faeth, T. L. Farias, and M. G. Carvalho (1995a), Fractal and projected structure properties of soot aggregates, *Combust. Flame*, *100*(4), 621–633.
Köylü, Ü. Ö., Y. Xing, and D. E. Rosner (1995b), Fractal morphology analysis of combustion-generated aggregates using angular light scattering and electron microscope images, *Langmuir*, *11*(12), 4848–4854.
Lewis, K., W. P. Arnott, H. Moosmüller, and C. E. Wold (2008), Strong spectral variation of biomass smoke light absorption and single scattering albedo observed with a novel dual-wavelength photoacoustic instrument, *J. Geophys. Res.*, *113*, D16203, doi:10.1029/2007JD009699.
Li, H., C. Liu, L. Bi, P. Yang, and G. W. Kattawar (2010), Numerical accuracy of "equivalent" spherical approximations for computing ensemble-averaged scattering properties of fractal soot aggregates, *J. Quant. Spectrosc. Radiat. Transfer*, *111*(14), 2127–2132.
Liu, C., R. L. Panetta, and P. Yang (2012), The influence of water coating on the optical scattering properties of fractal soot aggregates, *Aerosol Sci. Technol.*, *46*(1), 31–43.
Liu, C., Y. Yin, F. Hu, H. Jin, and C. M. Sorensen (2015), The effects of monomer size distribution on the radiative properties of black carbon aggregates, *Aerosol Sci. Technol.*, *49*(10), 928–940.
Liu, F., and G. J. Smallwood (2010), Radiative properties of numerically generated fractal soot aggregates: The importance of configuration averaging, *J. Heat Trans.*, *132*(2), 207–214.
Liu, F., C. Wong, D. R. Snelling, and G. J. Smallwood (2013), Investigation of absorption and scattering properties of soot aggregates of different fractal dimension at 532 nm using RDG and GMM, *Aerosol Sci. Technol.*, *47*(12), 1393–1405.
Liu, L., and M. I. Mishchenko (2005), Effects of aggregation on scattering and radiative properties of soot aerosols, *J. Geophys. Res.*, *110*, D11211, doi:10.1029/2004JD005649.
Liu, L., and M. I. Mishchenko (2007), Scattering and radiative properties of complex soot and soot-containing aggregate particles, *J. Quant. Spectrosc. Radiat. Transfer*, *106*(1), 262–273.
Liu, L., M. I. Mishchenko, and W. P. Arnott (2008), A study of radiative properties of fractal soot aggregates using the superposition T-matrix method, *J. Quant. Spectrosc. Radiat. Transfer*, *109*(15), 2656–2663.
Mackowski, D. W., and M. I. Mishchenko (1996), Calculation of the T matrix and the scattering matrix for ensembles of spheres, *J. Opt. Soc. Am. A*, *13*(11), 2266–2278.
Mackowski, D. W., and M. I. Mishchenko (2011), A multiple sphere T-matrix Fortran code for use on parallel computer clusters, *J. Quant. Spectrosc. Radiat. Transfer*, *112*(13), 2182–2192.
Martins, J. V., P. Artaxo, C. Liousse, J. S. Reid, P. V. Hobbs, and Y. J. Kaufman (1998), Effects of black carbon content, particle size, and mixing on light absorption by aerosols from biomass burning in Brazil, *J. Geophys. Res.*, *103*(D24), 32,041–32,050, doi:10.1029/98JD02593.
Mie, G. (1908), Beiträge zur Optik trüber Medien, speziell kolloidaler Metallösungen, *Ann. Phys.*, *330*(3), 377–445.
Mishchenko, M. I., and L. D. Travis (1998), Capabilities and limitations of a current FORTRAN implementation of the T-matrix method for randomly oriented, rotationally symmetric scatterers, *J. Quant. Spectrosc. Radiat. Transfer*, *60*(3), 309–324.
Mishchenko, M. I., L. D. Travis, R. A. Kahn, and R. A. West (1997), Modeling phase functions for dustlike tropospheric aerosols using a shape mixture of randomly oriented polydisperse spheroids, *J. Geophys. Res.*, *102*(D14), 16,831–16,847, doi:10.1029/96JD02110.
Mishchenko, M. I., B. Cairns, J. E. Hansen, L. D. Travis, R. Burg, Y. J. Kaufman, and E. P. Shettle (2004), Monitoring of aerosol forcing of climate from space: Analysis of measurement requirements, *J. Quant. Spectrosc. Radiat. Transfer*, *88*(1), 149–161.
Mishchenko, M. I., L. Li, and D. W. Mackowski (2013), T-matrix modeling of linear depolarization by morphologically complex soot and soot-containing aerosols, *J. Quant. Spectrosc. Radiat. Transfer*, *123*, 135–144.
Pandey, A., R. K. Chakrabarty, L. Liu, and M. I. Mishchenko (2015), Empirical relationships between optical properties and equivalent diameters of fractal soot aggregates at 550 nm wavelength, *Opt. Express*, *23*(24), A1354–A1362.
Reid, J. S., T. F. Eck, S. A. Christopher, P. V. Hobbs, and H. Brent (1999), Use of the Angstrom exponent to estimate the variability of optical and physical properties of aging smoke particles in Brazil, *J. Geophys. Res.*, *104*(D22), 27,473–27,489, doi:10.1029/1999JD900833.
Russell, P. B., R. W. Bergstrom, Y. Shinozuka, A. D. Clarke, P. F. DeCarlo, J. L. Jimenez, and A. Strawa (2010), Absorption Ångström exponent in AERONET and related data as an indicator of aerosol composition, *Atmos. Chem. Phys.*, *10*(3), 1155–1169.
Scarnato, B. V., S. Vahidinia, D. T. Richard, and T. W. Kirchstetter (2013), Effects of internal mixing and aggregate morphology on optical properties of black carbon using a discrete dipole approximation model, *Atmos. Chem. Phys.*, *13*(10), 5089–5101.
Schnaiter, M., C. Linke, O. Möhler, K. H. Naumann, H. Saathoff, and R. Wagner (2005), Absorption amplification of black carbon internally mixed with secondary organic aerosol, *J. Geophys. Res.*, *110*, D19204, doi:10.1029/2005JD006046.
Schuster, G. L., O. Dubovik, and B. N. Holben (2006), Angstrom exponent and bimodal aerosol size distributions, *J. Geophys. Res.*, *111*, D07207, doi:10.1029/2005JD006328.
Schuster, G. L., O. Dubovik, A. Arola, T. F. Eck, and B. N. Holben (2015), Remote sensing of soot carbon—Part 2: Understanding the absorption Angstrom exponent, *Atmos. Chem. Phys. Discuss.*, *15*(15), 20,911–20,956.
Smith, A. J. A., and R. G. Grainger (2014), Simplifying the calculation of light scattering properties for black carbon fractal aggregates, *Atmos. Chem. Phys.*, *14*(15), 7825–7836.
Smith, A. J. A., D. M. Peters, R. McPheat, S. Lukanihins, and R. G. Grainger (2015), Measuring black carbon spectral extinction in the visible and infrared, *J. Geophys. Res. Atmos.*, *120*, 9670–9683, doi:10.1002/2015JD023564.
Soni, K., S. Singh, T. Bano, R. S. Tanwar, and S. Nath (2011), Wavelength dependence of the aerosol Ångström exponent and its implications over Delhi, India, *Aerosol Sci. Technol.*, *45*(12), 1488–1498.
Sorensen, C. M. (2001), Light scattering by fractal aggregates: A review, *Aerosol Sci. Technol.*, *35*(2), 648–687.
Sorensen, C. M., and G. C. Roberts (1997), The prefactor of fractal aggregates, *J. Colloid Interf. Sci.*, *186*(2), 447–452.
Streets, D. G., S. Gupta, S. T. Waldhoff, M. Q. Wang, T. C. Bond, and Y. Bo (2001), Black carbon emissions in China, *Atmos. Environ.*, *35*(25), 4281–4296.
Toledano, C., V. E. Cachorro, A. Berjon, A. M. De Frutos, M. Sorribas, B. A. De la Morena, and P. Goloub (2007), Aerosol optical depth and Ångström exponent climatology at El Arenosillo AERONET site (Huelva, Spain), *Q. J. Roy. Meteorol. Soc.*, *133*(624), 795–807.
Ueda, S., K. Osada, and A. Takami (2011), Morphological features of soot-containing particles internally mixed with water-soluble materials in continental outflow observed at Cape Hedo, Okinawa, Japan, *J. Geophys. Res.*, *116*, D17207, doi:10.1029/2010JD015565.
Xu, Y. L. (1995), Electromagnetic scattering by an aggregate of spheres, *Appl. Optics*, *34*(21), 4573–4588.
Yang, M., S. G. Howell, J. Zhuang, and B. J. Huebert (2009), Attribution of aerosol light absorption to black carbon, brown carbon, and dust in China—Interpretations of atmospheric measurements during EAST-AIRE, *Atmos. Chem. Phys.*, *9*(6), 2035–2050.
Yang, P., K. N. Liou, L. Bi, C. Liu, B. Yi, and B. A. Baum (2015), On the radiative properties of ice clouds: Light scattering, remote sensing, and radiation parameterization, *Adv. Atmos. Sci.*, *32*, 1–32.

Yi, B., C. N. Hsu, P. Yang, and S. C. Tsay (2011), Radiative transfer simulation of dust-like aerosols: Uncertainties from particle shape and refractive index, *J. Aerosol Sci.*, *42*(10), 631–644.

Yi, B., P. Yang, and B. A. Baum (2014), Impact of pollution on the optical properties of trans-Pacific East Asian dust from satellite and ground-based measurements, *J. Geophys. Res. Atmos.*, *119*, 5397–5409, doi:10.1002/2014JD021721.

Yin, J. Y., and L. H. Liu (2010), Influence of complex component and particle polydispersity on radiative properties of soot aggregate in atmosphere, *J. Quant. Spectrosc. Radiat. Transfer*, *111*(14), 2115–2126.